ISET Journal of Earthquake Technology, Paper No. 565, Vol. 58, No. 3, September 2021, pp. 83-104

STOCHASTIC SIMULATION OF UTTARKASHI (1991) AND CHAMOLI (1999) EARTHQUAKES USING SPECIFIC BARRIER MODEL AND FUTURE EARTHQUAKES IN DELHI REGION

Hemant Shrivastava (Corresponding Author)
Assistant Professor, Civil Engineering Department
Madhav Institute of Technology & Science, Gwalior
Email id: *hemantshrivastava1986@mitsgwalior.in*

G.V. Ramana
Professor, Department of Civil Engineering
Indian Institute of Technology Delhi, Hauz Khas, New Delhi
E mail id: *ramana@civil.iitd.ac.in*

A.K. Nagpal
Former Dogra Chair, Department of Civil Engineering
Indian Institute of Technology Delhi, Hauz Khas, New Delhi
E mail id: *aknagpal_iitd@yahoo.co.in*

ABSTRACT

In this paper, a specific barrier model is calibrated to simulate ground motion in the Himalayan region. The Uttarkashi and Chamoli earthquakes are used to estimate the seismic parameters of the source model. Key seismic parameters are global stress drop and local stress drop. The parameters are estimated for κ_o and f_{max} filters. The local stress drop values for the two filters are different but simulate ground motion for the two filters are close. The simulated ground motions with estimated seismic parameters are compared with the observed ground motion for the Chamoli earthquake in the Delhi region and show closer results than predict ground motion using the stochastic finite fault method. The estimated seismic parameters are then used to simulate the future great earthquakes (M_w 7.5, 8.0, and 8.5) in the Delhi region at bedrock level from the central seismic gap of the Himalayan region.

KEYWORDS: Himalaya Region; Delhi Region; Specific Barrier Model; Global Stress Drop; Local Stress Drop

INTRODUCTION

The Himalayan region is one of the most active inter-plate seismic region in the world. The collision between the Indian plate and Eurasian plate produced major thrust faults: the Main Boundary Thrust (MBT), the Main Central Thrust (MCT), and the Himalayan Frontal Thrust (HFT), two former faults are shown in Figure 1, which contributes significantly in the tectonic activities in the Himalaya region (Rajendra and Rajendran [1]). The Himalayan region has experienced several great earthquakes in the past hundred years (1803 Kumaon; 1833 Kathmandu; 1905 Kangra; 1934 Bihar-Nepal; 1950 Assam). In the past two decades, three moderate earthquakes (Uttarkashi, 1991; Chamoli, 1999; Sikkim, 2011) occurred in the Himalayan seismic belt causing extensive damage in nearby areas. In the last decade, earthquakes of small to moderate magnitude (M_w = 3-5.7) occurred in the Himalayan seismic belt. A 500 to 800 km long segment of the north-western Himalayan region between the rupture zones of the Kangra earthquake (1905) and Bihar-Nepal (1934) earthquake has been recognized as a seismic gap and called as “Central Seismic Gap” is shown in Figure 1. It has been interpreted to have a potential slip for generating future great earthquakes (Rajendran and Rajendran [1], Khattri and Tyagi [2], Khattri [3]). Feld and Bilham [4] studied the earthquakes between the periods 1833-1934 and suggest that a major earthquake can be followed by a great earthquake at the same location. The seismic activity in the Himalayan region arises from the movement of the Indian plate where it descends beneath the Tibetan plateau. The convergence rate and differential shortening rate from GPS observations (Feld and Bilham [4]) and average slip deficit (Bilham and Ambraseys [5], Bilham and Wallace [6]) between the Indian plate and Tibetan plateau support the continuing seismic activity in the Himalayan region. The 100 years probability of occurrence of the great earthquake (M_w 8.5) in the central seismic gap is about 0.52 (Khattri [7]). Mondal et al. [8] studied the GPS deformation measurements and found that the region lying between latitude 29°N-30°E and 79°N-80°E has high strain accumulation and less seismic activity, and identified this region as a zone of a future large earthquake. The central part of the Himalayan region can expect a great earthquake in the immediate future (Bilham et al. [9], Bilham and Ambraseys [6]).

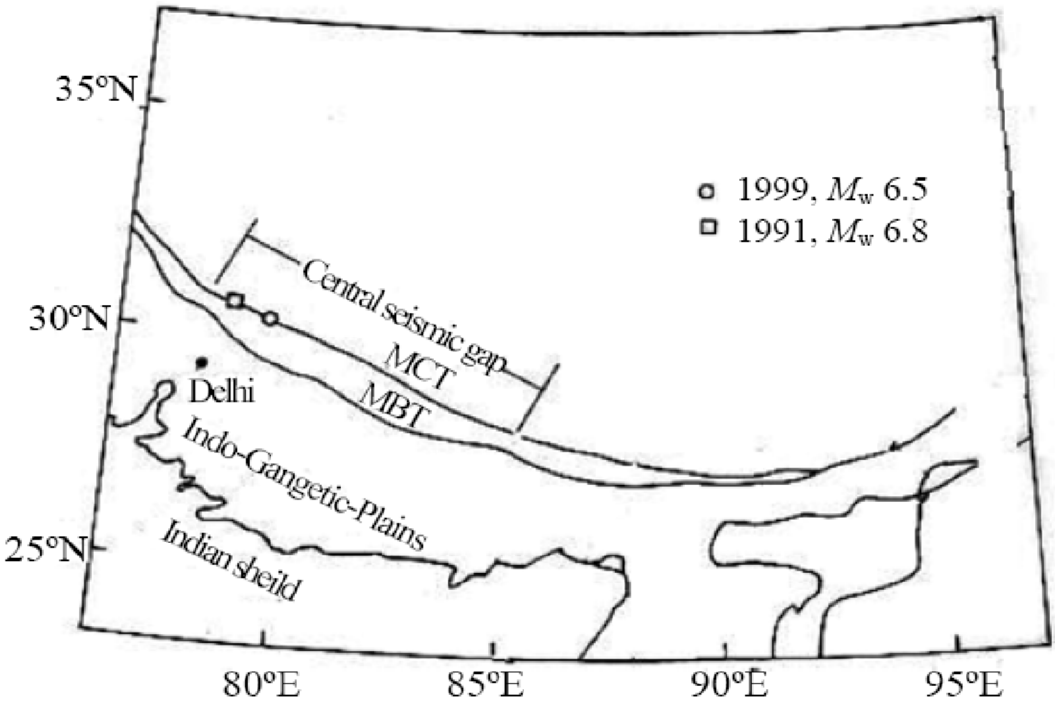

Fig. 1 Tectonic map of the Himalayan region

Several studies (Singh et al. [10], Joshi [11], Anbazhagan et al. [12], Harbindu et al. [13], Harbindu et al. [14], Sharma et al. [15], Mittal and Kumar [16], Chopra et al. [17], Yu et al. [18], Mohan and Joshi [19]) have been conducted relating to the simulation of Himalayan earthquakes (Dharamsala, 1986; Uttarkashi, 1991; Chamoli, 1999; Uttarakhand-Nepal Border, 2011). Different methodologies have been used to simulate ground motion: stochastic simulation (Harbindu et al. [13], Harbindu et al. [14]), composite source model (Yu et al. [18]), empirical green function (Sharma et al. [15]), stochastic finite fault modeling technique (Singh et al. [10], Chopra et al. [17], Anbazhagan et al. [12], Mittal and Kumar [16]) and semi-empirical technique (Joshi [11], Mohan and Joshi [19]).

In the Delhi region, no records of potential future great earthquakes (M_w> 8.0) are available. Singh et al. [10] have simulated strong ground motion in the Delhi region from future great earthquakes in the central seismic gap of the Himalayan region using the stochastic finite fault simulation method (Bresenev and Atkinson [20]) and observed the peak ground acceleration varies from 17 to 52 gal at ridge observatory (hard soil) and 174 gal and 218 gal at soft sites. In the finite fault simulation method, the fault plane is divided into sub-faults and each sub-fault acts as a point source. The radiation from an earthquake is obtained as the sum of contributions from all sub-faults. The time series from each sub-fault is based on the ω^2 model (Beresnev and Atkinson [20]). Despite its popularity in the simulation of ground motion, the fundamental problem with the ω^2 model is the ambiguous nature of the stress drop (Boore and Atkinson [21], Papageorgiou [22]). It is pointed out by Beresnev [23], that the stress drop is a poorly defined source parameter and does not quantify the actual stress change during an earthquake, and its values derived from the seismic spectra have little physical meaning.

The specific barrier model for simulating the source spectrum proposed by Papageorgiou and Aki [24, 25] is free from the disadvantage of the point source model (Halldorsson and Papageorgiou [26], Papageorgiou [27]). It allows consistent ground motion simulation over the entire frequency range and for all distances of engineering interest. This model can be applied in the far-field region and near-fault region (Papageorgiou [27]) and is a better representation of the faulting process. The model involves two key parameters (1) global stress drop that relates to the entire fault and (2) local stress drop that relates to the local sub-fault in the fault.

Therefore, the specific barrier model has been used for the simulation of the Uttarkashi and Chamoli earthquakes. In this present study, the global stress drop and local stress drop parameters of the specific barrier model are calibrated with the recorded data for Uttarkashi and Chamoli earthquakes. The data recorded at 23 stations of two earthquakes in the Himalayan region and the genetic algorithm method for calibration of stress drop (global and local) parameters has been used. Further, the calibrated specific barrier model for Uttarkashi and Chamoli earthquakes has been used for simulating the future great earthquake (M_w 7.5, 8.0, 8.5) at the bedrock level in the Delhi region (Shrivastava [28]). The results are discussed in terms of peak ground acceleration (PGA) and spectral acceleration (*Sa*) response spectra.

SEISMICITY OF HIMALAYAN REGION

The Himalaya region is characterized by three major thrust systems Main Central Thrust (MCT), Main Boundary Thrust (MBT), and Himalaya Frontal Fault (HFF) are developed due to the collision of the Indian Plate with the Eurasian plate and partition the region into three geologically and topographically distinct regions (Figure 2) (Valdiya [29]). The region to the north of the MCT is composed of highly metamorphosed rocks, which form the higher Himalaya. The region between the MCT and MBT is made up of meta-sediments and is known as the lesser Himalaya. The region south of MBT and up to HFF is composed of an unconsolidated Siwalik system of Neogene sediments and is designated as Outer Himalaya. Further south of HFF lay the plains of the Ganges. The interpolate thrust zone, a part of a detachment that separates the underthrusting Indian plate from lesser Himalayan, indicates that the MBT rather than the MCT is the most active structure of the Himalayan arc and suggested that the great Himalayan earthquakes (M_w> 8) on this detachment plane (Ni and Barazangi [30]). The hypocentres of Uttarkashi (1991) and Chamoli (1999) earthquakes are lies on the plane of detachment (Kayal [31]). This region lies between the rupture zones of the 1905 Kangra earthquake and the 1934 Bihar Nepal earthquake.

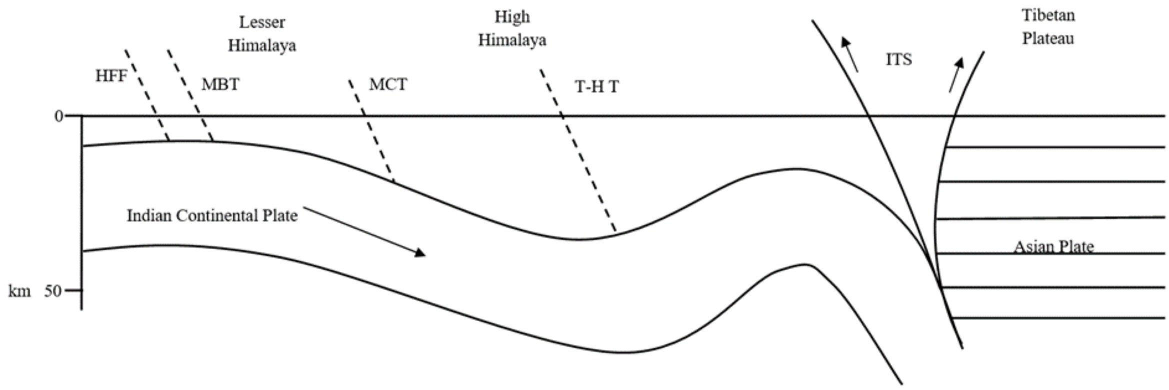

Fig. 2 Cross-section of Himalaya showing the tectonic (HFF- Himalaya Frontal Fault; MBT- Main Boundary Thrust; MCT- Main Central Thrust; T-HT- Trans-Himadri Thrust; ITS- Indus-Tsangpo Suture)

STRONG GROUND MOTION DATABASE

The data consist of 46 horizontal records of the Uttarkashi and Chamoli earthquakes obtained from a strong motion network of 23 analog accelerographs (SMA-1) deployed in the Garhwal and Kumaon Himalaya in 1991 by the Department of Earthquake Engineering, University of Roorkee (Now IIT Roorkee). In the Delhi region, the three sites at which accelerograms of the mainshock of the Chamoli earthquake are recorded by accelerographs deployed by CBRI, Roorkee are (1) CPCB, Arjun Nagar; (2) IHC, Lodhi Road, and (3) CSIR, Rafi Marg. Also, recorded at Ridge Observatory (RO) site by IMD. The CPCB, IHC, and CSIR sites are situated on soft soil and RO lies on hard rock (Singh et al. [10]).

SPECIFIC BARRIER MODEL

The stochastic modeling method (Boore [32]) has been used for the simulation of ground motion. The Fourier amplitude spectrum of shearwaves of horizontal strong ground motion, $Y(M_o, R, f)$, at a distance R from a source, can be expressed as

$$Y(M_o, R, f) = E(M_o, f)G(R)A_n(f)P(f) \tag{1}$$

$$E(M_o, f) = c * S(M_o, f) \tag{2}$$

where c is constant, $S(M_o, f)$ is source spectrum, $G(R)$ is path effects, $A_n(f)$ is path attenuation term, $P(f)$ is site terms, M_o is the seismic moment, f is the frequency and R represent distance in km.

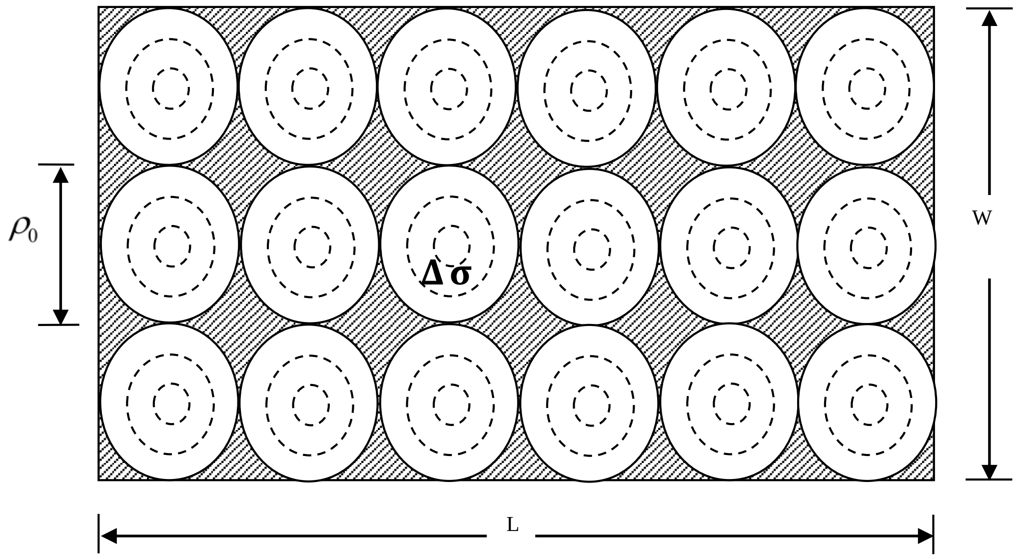

Fig. 3 Schematic view of specific barrier model (Papageorgiou and Aki [24])

In the specific barrier model, the heterogeneous seismic fault plane is assumed as a rectangular fault plane of length L and width W and divided into the circular crack, of equal radius ρ_o, which represents the subevent as shown in Figure 3. The rupture front sweeps over the fault plane, the rupture nucleates at the center and spread radially with constant rupture velocity, and stops abruptly at a distance equal to the radius of each crack. The radiation of elastic waves emitted from each crack as its breaks is based on a physical description of source processes by using kinematic dislocation theory (Aki and Richards [33]). The global stress drop represents the size of the entire main source and controls the lower frequencies. The local stress drop is the stress drop on each subevent that composes earthquake events. The subevents are assumed to break randomly and independently. The acceleration source spectrum (Papageorgiou [22]), the sum of high-frequency ground motion from each subevent, is expressed as follows

$$S(M_o, f) = (2\pi f)^2 \left\{ N\left[1 + (N-1)\left(\frac{\sin(\pi f T)}{(\pi f T)}\right)^2\right]\right\}^{\frac{1}{2}} \bar{M}_{oi}(f) \tag{3}$$

$$\bar{M}_{oi}(f) = \frac{M_{oi}}{1 + \left(\frac{f}{f_2}\right)^2} \tag{4}$$

where $M_{oi}(f)$ is the acceleration source spectrum of the individual subevent, and N is the total number of subevents that compose the rupture.

The high-frequency radiation from each subevent of the specific barrier model sums up incoherently and their spectrum is described by Equation (1). $M_{oi} = (16/7)\Delta\sigma_L \rho_o^3$ is the seismic moment released by the crack and the patch corner frequency f_2 is corresponding to the crack radius, ρ_0, by $f_2 = \dfrac{C_s \beta}{2\pi\rho_o}$ where β denotes the source region S-wave velocity, C_s is an increasing function of the υ/β ($1.72 \leq C_s \leq 1.85$for $0.7 \leq \upsilon/\beta \leq 0.9$) (Aki and Richards [33]) and υ indicate the propagating rupture velocity inside the circular cracks. The faulting duration, T, is related to the corner frequency f_1 by $T = C/f_1$, in which C is a model-dependent constant. In this study, $C = 0.47$ is selected (Papageorgiou [22]). The size of the sub-fault is not optional and may be estimated from the empirical relationship (Halldorsson and Papageorgiou [26]). In this study, the empirical relationship between the moment of target event (M_w) and the size of sub-fault is derived from the following relation

$$\log 2\rho_o = -2.58 + 0.5 M_w \tag{5}$$

which is a region-independent relationship and may be employed worldwide (Halldorsson and Papageorgiou [26], Beresnev and Atkinson [34]).

$\Delta\sigma_G$ is the global stress drop of the main event and $\Delta\sigma_L$ is the local stress drop of the subevent. The source term E(M_0, f) may be computed as a product of S(M_0, f) by a frequency-independent scaling factor of $c = \dfrac{FSR_{\phi\theta}V}{4\pi\rho\beta^3}$ where $R_{\phi\theta}$ is used to account for the average S-wave radiation pattern, FS denotes the free surface amplification, V indicates the partitions of the total S-wave energy into two horizontal components. The ρ and β represent the mass density and the S-wave velocity surrounding the source region, respectively. The anelastic whole path attenuation factor includes all the losses which have not been accounted for by the geometrical attenuation factor. The path attenuation factor is expressed as $A_n(f) = \exp\left(-\dfrac{\pi f R}{\beta Q(f)}\right)$(Boore and Atkinson [21]). $Q(f)$is the quality factor, which includes both anelastic absorption and scattering. $G(R)$ is the geometrical spreading term (Singh et al. [10]) which may be taken as

$$G(R) = \begin{cases} R^{-1} \; for\, R \leq R_x \\ (RR_x)^{-1/2} \;\; for\, R > R_x \end{cases} \tag{6}$$

In this study, R_x has been taken as 100 km. The site term is considered to be independent of the source-to-site travel distance.

To account for site amplification and diminution effects, Boore [32] suggested separating terms into amplification *(A (f))* and attenuation *(D (f))* follows as

$$P(f) = A(f)D(f) \tag{7}$$

A(f) is the frequency-dependent amplification function, which accounts for the amplification of the waves due to the local site effect. The factor *D(f)* accounts for the path-independent loss of high frequency in the ground motion. Two filters κ_o and f_{max} chosen as diminution factor and is given by the following equation (Boore [32])

$$D(f) = \exp(-\pi k_o f) \tag{8}$$

$$D(f) = \left[1 + (f/f_{\max})^8\right]^{-1/2} \tag{9}$$

SITE AMPLIFICATION

The topography and local soil conditions can significantly modify the ground motion. The amount of amplification depends on factors are the thickness of the soil layer, degree of compaction, and age, which influence the shear wave velocity, density and damping characteristics of the soil. Many studies have been conducted to estimate site effects (Borcherdt [35], Nakamura [36], Lermo and Chaveza-Garcia [37], Motazedian [38]). The site effects are estimated by dividing the spectrum obtained at the target site by that obtained at a nearby reference site, which is preferably on the bedrock, standard spectral ratio (*SSR*) technique (Borcherdt [35]). However, it is difficult to find a convenient ideal reference site to be available nearby the target site (Stiedl et al. [39]). Lermo and Chavez-Garcia [37] proposed a methodology to compute site effects without a reference site, which involves dividing the horizontal component of the shear wave spectrum by the vertical component at the site, the horizontal to vertical ratio (*H/V*) technique. To compute the site effect, the acceleration time history of each recording station is the window for a time length of 10 sec with an arrival time of the shear wave. A cosine taper is applied to the time windowed data. The obtained time history is transformed into the frequency domain. The obtained Fourier spectra are smoothed using five-point smoothing algorithms. In the Himalayan region, the *H/V* ratios are estimated using the S-wave portions of records of the Chamoli earthquake aftershocks and low magnitude earthquakes listed in Table 1. Figure 4 shows the mean amplification function (*H/V*) for the rock site.

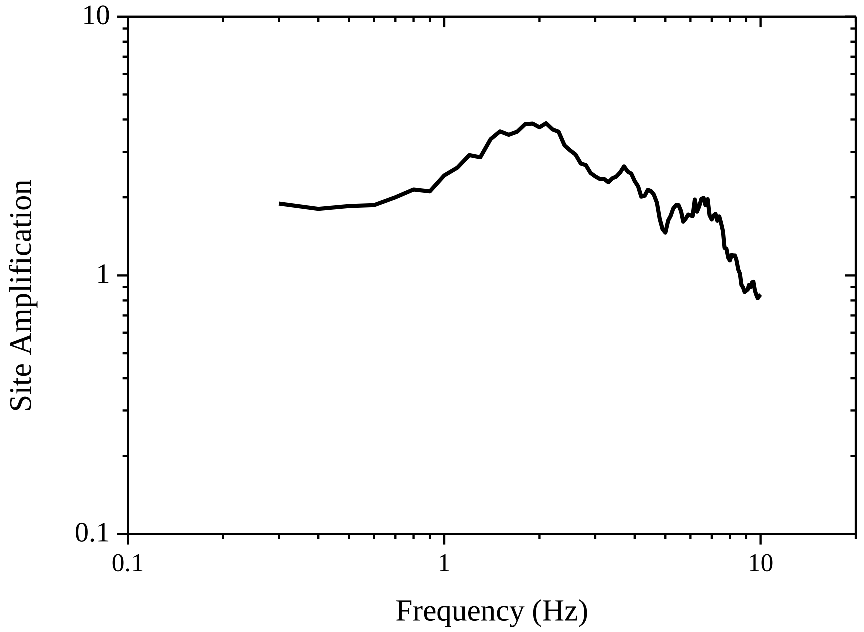

Fig. 4 Site amplification function for rock sites in Himalaya region

Table 1: Detail of the Chamoli earthquake aftershock and smaller magnitude earthquakes in Gharwal Himalaya used for estimate site amplification (Harbindu et al. [13])

Event (yymmdd-hhmm)	Latitude (^{0}N)	Longitude (^{0}E)	Focal Depth (km)	Magnitude (M_b)
990328-1936	30.32	79.39	10	5.4
990329-1320	30.29	79.29	10	4.6
990330-2103	30.38	79.33	10	5.3
990406-3041	30.33	79.32	10	5.1
990407-2046	30.25	79.32	10	4.7
990507-1712	30.11	79.35	10	4.5
051014-0709	30.90	78.30	10	5.2
090225-0404	30.60	78.30	10	3.7
090318-11:22	30.90	78.20	10	3.3
090515-1839	30.50	78.30	15	4.1
100501-2233	29.90	80.10	10	4.6
100503-1715	30.40	78.40	8	3.5

In the Delhi region, *SSR* and *H/V* techniques have been used to estimate the site amplification at different stations during the Chamoli earthquake are compared in Figure 5. Among four sites in the Delhi region, the Ridge Observatory site is located on a rock site. Hence site effects are estimated with respect to the Ridge observatory (Singh et al. [10]). The site amplification for *SSR* and *H/V* and observed that the *H/V* technique underestimate the site amplification. From literature (Castro et al. [40], Shoja-Taheri and Gofrani [41]), it found that the *H/V* technique underestimates site amplification. Hence, for simulation of ground motion in Delhi considered results given by *SSR*.

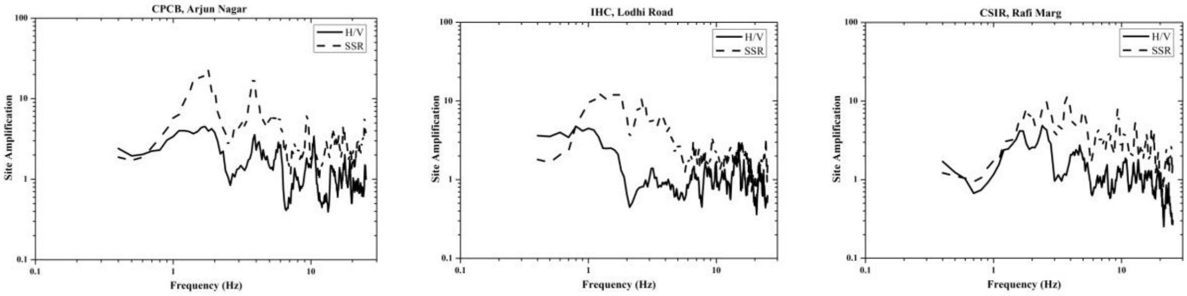

Fig. 5 Comparison between site amplification factors estimated by SSR and H/V techniques, at the recorded station in the Delhi region during the Chamoli earthquake

GENETIC ALGORITHM

Genetic algorithm (GA) is a stochastic optimization method to search for near-optimum solutions and is based on Darwin's natural evolution laws (Holland [42]). The GA procedure involves a reproduction process comprising of three operations: (i) selection, (ii) crossover, and (iii) mutation to produce better offspring to achieve a solution close to the fitness function (Goldenberg [43]). In the simulation of ground motion, GA has been effectively utilized for the calibration of the seismological model (Soghart et al. [44], Zafarani et al. [45]), generation of attenuation relationship (Yilmaz [46]), and scaling of ground motion (Naeim et al. [47]).

GA starts with a random initial set of solutions, called population. Individuals in the population are called chromosomes, which are probable solutions to the problem. Chromosomes are sets of binary strings. The fitness function is evaluated for an initial set of solutions. Selection operator is used for the selection of individuals based on the fitness value. The individual with a lower fitness value has more chance to be selected for the next generation with respect to the individual with the highest fitness value. After the selection of individuals from the population, offspring chromosomes are produced by combining two parent chromosomes using a crossover operator. This simplest crossover method is illustrated in Figure 6. The number of crossovers is determined by crossover probability and up to 80% give satisfying outcomes in many applications (Coley [48]). In mutation operator, changing a randomly selected bit among all chromosomes from 1 to 0 or 0 to 1 is shown in Figure 7, preventing premature loss of genetic information from the population. Mutation probabilities of 1-2% are preferred to satisfy the stability of the population (Gen and Cheng [49]). After completion of the above operations, the population consists of a combination of old and new individuals. The process of reproduction continues generation after generation until new generations achieved lower fitness value than older generations.

Cut-off

Point

Parent 1:	1101	0100
Parent 2:	1001	0111
Offspring 1:	1101	0111
Offspring 2:	1001	0100

Fig. 6 Crossover operation

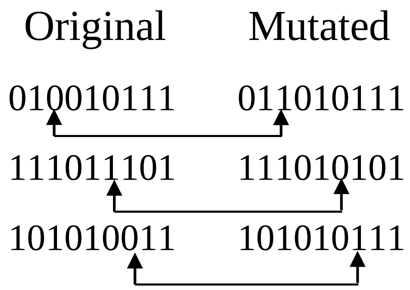

Fig. 7 Mutation operation

CALIBRATION AND RESULTS

In the specific barrier model, the most important parameters represented by vector θ are $\Delta\sigma_G$ and $\Delta\sigma_L$ which control the Fourier spectra at lower and higher frequencies (Halldorsson and Papageorgiou [26]). As the pseudo-spectral velocity (*PSV*) is the characteristic of ground motion and it quantifies the demand of earthquake on the structures. These model parameters are calibrated through a comparison of observed and simulated *PSV*. The $\Delta\sigma_G$ and $\Delta\sigma_L$ are varied to simulate the *PSV* at the observed station. For a given set of θ, the measure of error between the observed and simulated ground motion is defined as (Halldorrson and Papageorgiou [26])

$$e(\theta) = \log\left(\frac{y}{\mu(\theta)}\right) \tag{10}$$

where y = *PSV* of observed ground motion and $\mu(\theta)$ = *PSV* of simulated ground motion. If the error between observed and simulated is greater than 1.0 imply under prediction of observed values and less than 1.0 implies over prediction of values.

The best model parameters θ are obtained by minimizing the norm (Γ) given by

$$\Gamma = \sqrt{\sum_{i}^{N_e}\sum_{j}^{n_i n_j}\left[e_{ij}(\theta)\right]^2} \tag{11}$$

where N_e is the number of earthquake events considered in the analysis, n_i represents the number of observation stations (i.e. the number of geometric mean *PSV* data) and n_j represents the number of discrete oscillator frequencies (f).

For minimization, the GA optimization technique (Goldenberg [43]) has been used. In this study, n_j = 12 has been chosen (f = 0.5, 0.7, 0.9, 1.1, 1.5, 2.0, 2.6, 3.4, 4.4, 5.8, 7.6 and 10.0 Hz) (Halldorsson and Papageorgiou [26]). In GA individual population selection is based on the principle of survival of the fittest. Crossover and mutation operators are controlled by providing each chromosome with random probabilities for crossover and mutation. The best individuals are selected from old generation populations and the roulette wheel selection is used to choose parents proportional to their fitness function. Single point crossover is performed at a crossover point for the chosen parents to generate new individuals in the next generation. Figure 8 illustrated the procedure for calibration of a specific barrier model using GA. The norm (Equation 11) is used as the fitness function. The fitness function is estimated for individual sets of the initial population of $\Delta\sigma_G$ and $\Delta\sigma_L$ values. The GA search was carried out with a population of 40 models, for 250 generations, with a crossover probability is 50% and mutation probability is 1%. To confirm the minimum global would be found, the GA search process has been run 10 times with different initial populations.

The f_{max} and κ_o filters are generally used in the stochastic modeling of ground motion. Halldorsson and Papgeorgiou [26] used the κ_o filter with SBM instead of the f_{max} filter since the κ_o filter gave a better fit to their data. In the present study, the calibration of SBM has been carried out for f_{max} and κ_o filters. The seismological parameters for the simulation of Uttarkashi and Chamoli earthquakes, other than $\Delta\,\sigma_G$ and $\Delta\,\sigma_L$ values are given in Table 2.

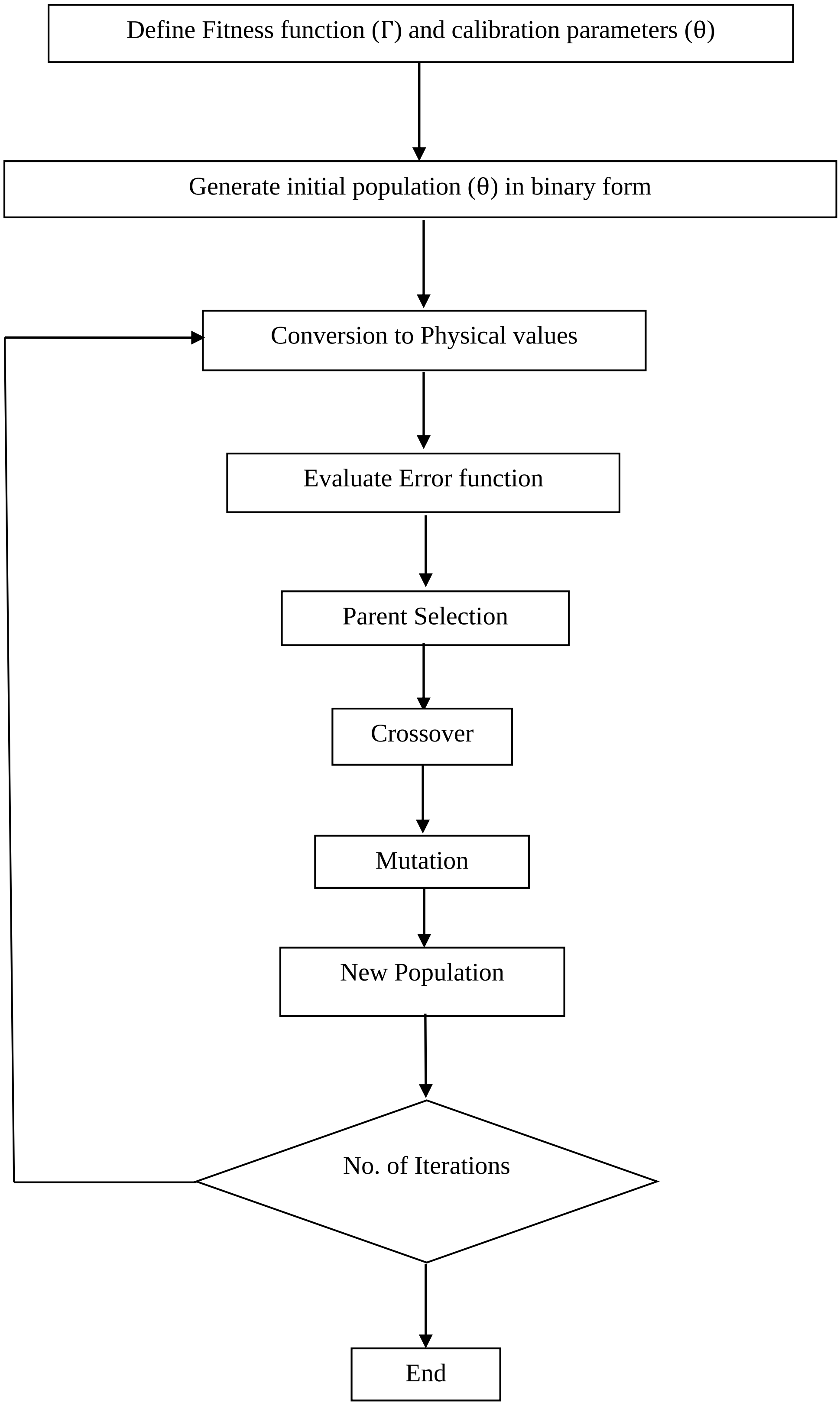

Fig. 8 Procedure for calibration of the specific barrier model

Table 2: Seismological parameters used in the calibration for global and local stress drop parameters of the specific barrier model

Parameters	Values
$F, V, R_{\theta\phi}$	2, 0.71, 0.55
Crustal density (kN/m^3)	2.85
Rupture velocity (km/sec)	3.6
Geometrical spreading	$G(R) = R^{-1}$ for $R \leq R_x$ $G(R) = (RR_x)^{-1/2}$ for $R > R$
$Q(f) = Q_0 f^n$	$508 f^{0.48}$
f_{max} (Hz)	15
κ_o	0.05

Table 3: Comparison between $\Delta\sigma_L$ and Γ for different $\Delta\sigma_G$ and two filters

$\Delta\sigma_G$	f_{max} filter		κ_o filter	
	$\Delta\sigma_L$	Γ	$\Delta\sigma_L$	Γ
30	179	6.361557	512	6.449859
40	175	6.438932	480	6.748296
50	175	6.516576	420	6.961143
60	195	6.543423	410	7.091167
70	195	6.573330	370	7.183412
80	190	6.601835	385	7.252429
90	205	6.615902	390	7.299583
100	200	6.643134	385	7.339821

In literature (Singh et al. [10], Harbindu et al. [13], Yu et al. [18], Joshi [50], Kumar et al. [51], Sriram and Khattri [52]), it has been seen that the value of stress drop varies from 30 to 100 bars for Uttarkashi and Chamoli earthquakes. Hence, the variation of global stress drop values at the source between 30 to 100 bars has been considered. Initially, the GA search scheme was applied using $\Delta\sigma_L$ as the variable for calibration for both earthquakes taken together. The $\Delta\sigma_L$ value and Γ value estimated for $\Delta\sigma_G$ (30, 40, 50, 60, 70, 80, 90, and 100 bars) for f_{max} and κ_o filters are given in Table 3. It has been seen that the fitness function value is lowest for $\Delta\sigma_L$ = 179 bars for the f_{max} filter.

From calibration using $\Delta\sigma_G$ and $\Delta\sigma_L$ as variables, the optimum evaluated $\Delta\sigma_G$ and $\Delta\sigma_L$ values for both earthquakes taken together are 30 bars and 180 bars for the f_{max} filter and 30 bars and 510 bars for the κ_o filter. $\Delta\sigma_L$ obtained from the two filters are quite different from the value obtained from the κ_o filter about 2.8 times the value from the f_{max} filter. The *Sa* for the simulated ground motion for f_{max} and κ_o are compared in Figure 9. Two stations (Bhatwari and Uttarkashi) for the Uttarkashi earthquake and two stations (Gopeshwar and Tehri) for the Chamoli earthquake have been selected for comparison. It is observed that although $\Delta\sigma_L$ values are quite different for the two filters, the corresponding simulated response spectra differ only marginally. The root means square errors of $e(\theta)$between response spectra for simulated and observed ground motion considering all the 23 stations for two filters are evaluated to be 0.423 and 0.523 for the f_{max} filter and κ_o filter respectively. For further study f_{max} filter has been chosen.

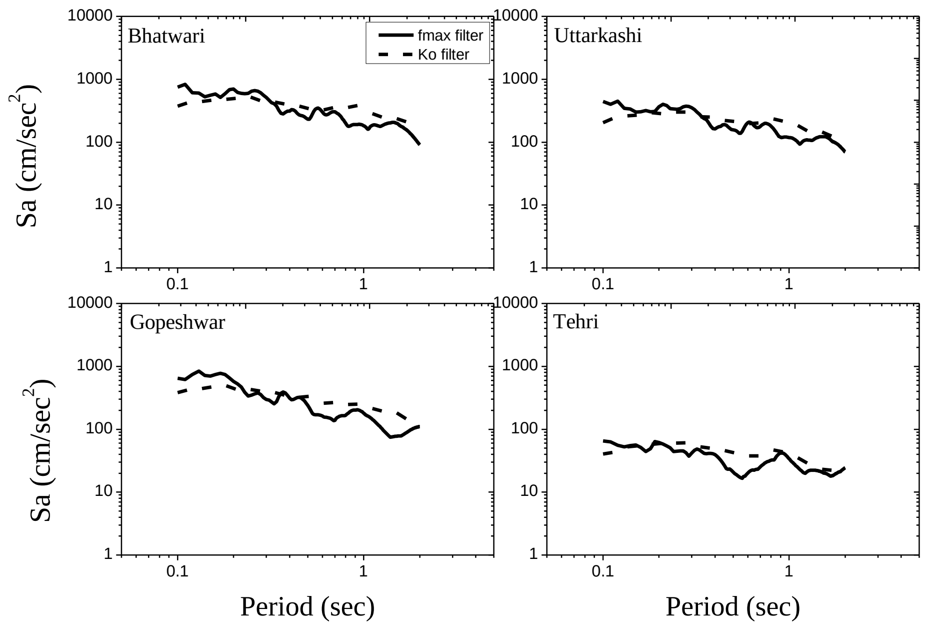

Fig. 9 Comparison of simulated *Sa* (5% damping) for two filters (a) Uttarkashi earthquake (Station- Bhatwari and Uttarkashi) (b) Chamoli earthquake (Station- Gopeshwar and Tehri)

A comparison of the *Sa* (5% damping) for observed and simulated ground motion at various stations for the Uttarkashi and Chamoli earthquakes is shown in Figure 10 and 11 respectively. It is observed that the simulated *Sa*-period trend is similar to the observed *Sa*-period trend. $\Delta \sigma_G$ obtained using combined recorded data of both Uttarkashi and Chamoli earthquakes in the SBM is compared with the stress drop values from various other models obtained using either Uttarkashi or Chamoli earthquake recorded data in Table 4. Significant variation in stress drop values is observed.

Table 4: Comparison of stress drop values

Model	**Source of recorded data**		
	Uttarkashi EQ	**Chamoli EQ**	**Uttarkashi & Chamoli EQ**
Specific barrier model	-	-	30 bars
Yu et al. [18]	30 bars	-	-
Sriram and Khattri [57]	40 bars	-	-
Singh et al. [10]	-	60 bars	-
Joshi [50]	77 bars	29 bars	-
Harbindu et al. [13]	33 bars	105 bars	-

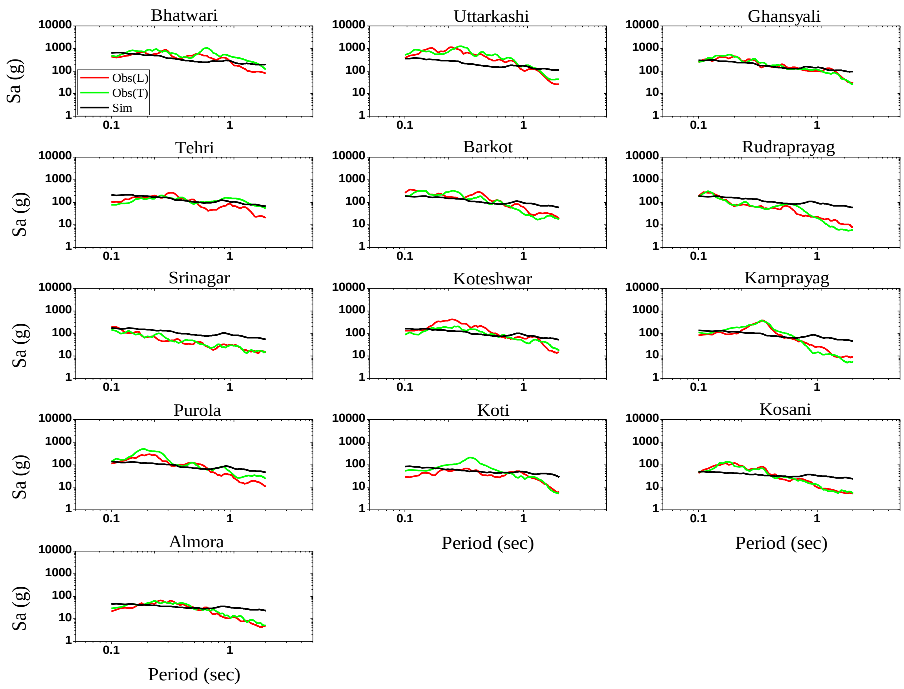

Fig. 10 Comparison of *Sa* (5% damping) for observed and simulated ground motion at various stations of Uttarkashi earthquake

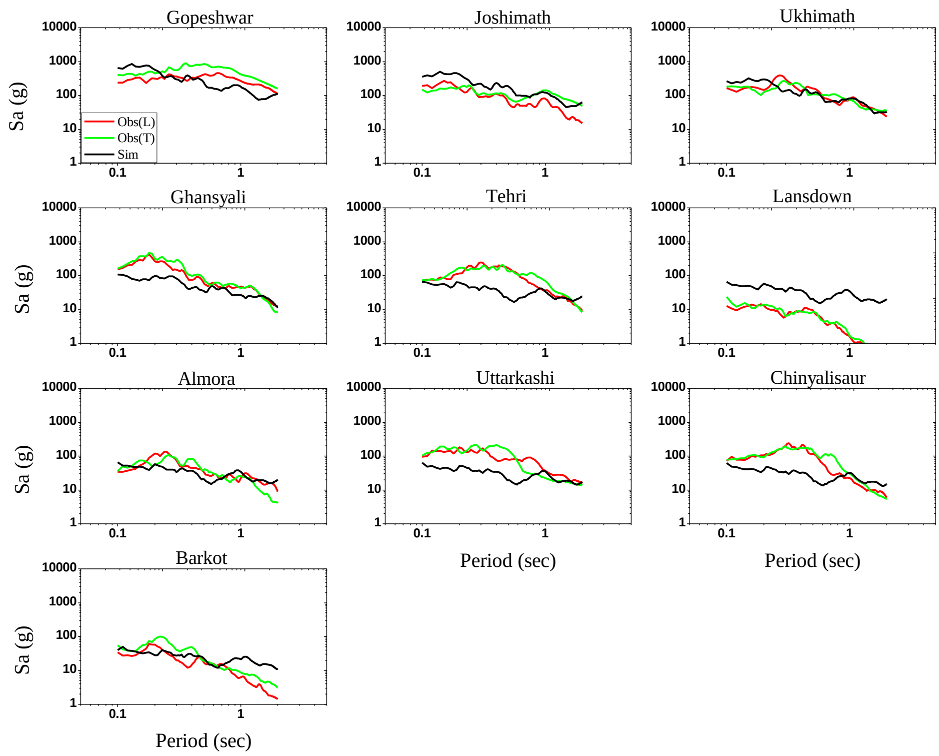

Fig. 11 Comparison of *Sa* (5% damping) for observed and simulated ground motion at various stations of Chamoli earthquake

Also, the comparison of *PGA* for observed and simulated ground motion with hypocentral distance for Uttarkashi and Chamoli earthquakes is shown in Figure 12. The trend of decay of simulated *PGA* values with hypocentral distance is similar to observed *PGA* values. The difference in observed and simulated *Sa* and *PGA* values may largely be attributed to local site effects. The distribution of the measure of error with hypocentral distance at chosen *f* for Uttarkashi and Chamoli earthquakes is shown in Figure 13. No strong pattern with hypocentral distance is observed.

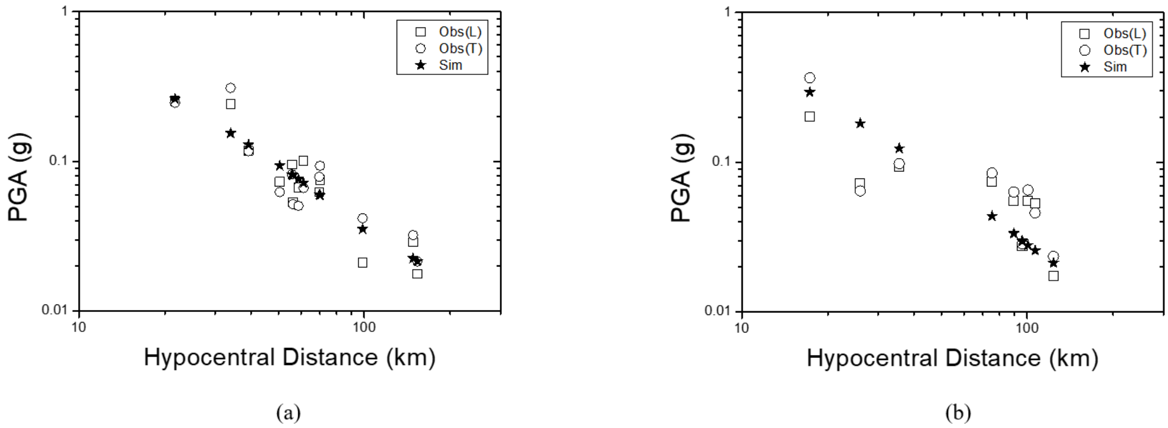

Fig. 12 Comparison of PGA for observed and simulated ground motion with hypocentral distance for (a) Uttarkashi earthquake and (b) Chamoli earthquake

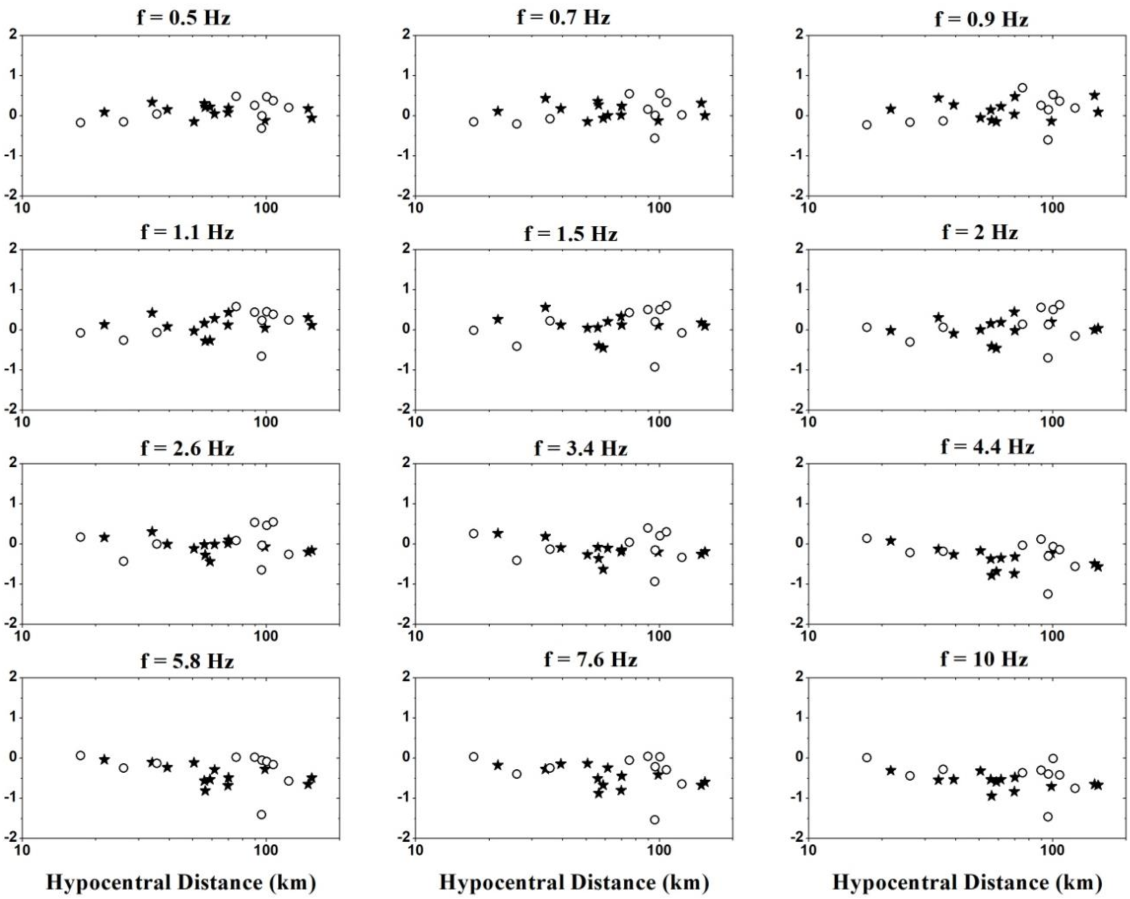

Fig. 13 Distribution of error for Uttarkashi earthquake (*) and Chamoli earthquake (o) with hypocentral distance

The model bias is defined as the average of $e(\theta)$ between the observed and simulated PSV, taken over all stations (Bresnev and Atkinson [34]). The mean and standard deviation of $e(\theta)$ at different *f* for

Uttarkashi and Chamoli earthquakes is shown in Figure 14. It is observed that the *e(θ)* lies in a narrow band at all *f*.

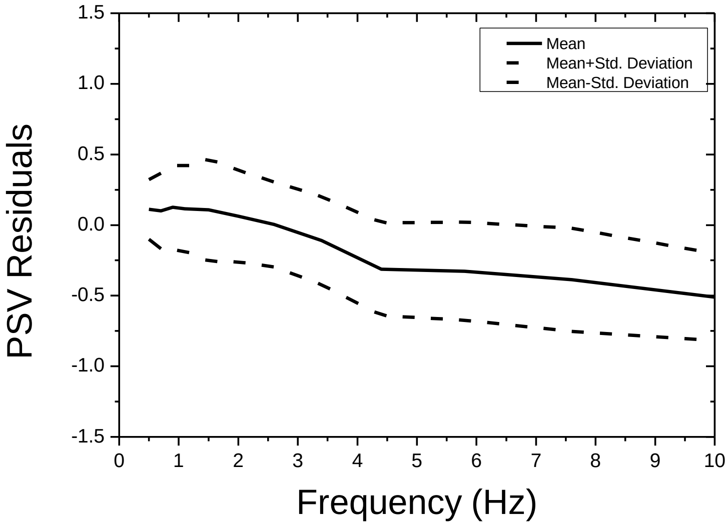

Fig. 14 Mean and standard deviation of PSV residuals at different frequencies for Uttarkashi and Chamoli earthquakes

Since the estimated values of $\Delta\sigma_G$ and $\Delta\sigma_L$ and other parameters used for simulation of ground motion result in *Sa*- period trend and *PGA*-hypocentral distance trend and differences between the observed and the simulated values of *Sa* and *PGA* may be ascribed to local site effects, therefore, these parameters may be used to generate future great earthquake in the central seismic gap of Himalaya region.

GENERATION OF STRONG GROUND MOTION DUE TO FUTURE GREAT EARTHQUAKES IN DELHI REGION AT BEDROCK LEVEL

For the simulation of the future great earthquakes (M_w 7.5, 8.0, 8.5) in the Delhi region, the location of the fault plane and hypocenter of one of the future earthquakes is assumed between MBT and MCT, centered at 30.0°N, 79.2°E. The location of the other future earthquake (Singh et al. [10]) is the same as for the Chamoli earthquake in the Himalayan Region. For the validation of simulated ground motion in the Delhi region, recorded data at sites CPCB, IHC, CSIR, and RO during the Chamoli earthquake are made used. The simulated *PGA* values using a specific barrier model for the f_{max} filter are compared with observed *PGA* (Longitudinal component, L; Transverse component, T; Geometric Mean, GM) values in Table 4. The *PGA* value predicted using the stochastic finite fault method (Singh et al. [10]) is also included in Table 5. It observed that simulated values obtained using a specific barrier model are closer to the observed values than the values obtained using the stochastic finite fault method at two of the four sites, namely CPCB and IHC sites. More recorded data would need to be available to ascertain the efficacy of various simulation procedures.

Table 5: Comparison of observed and simulated PGA (cm/sec^2) values in the Delhi region

Station	Observed			Simulated	
	L	T	GM	Present Study	Singh et al. [10]
CPCB	11.92	15.292	13.50	13.06	12.2
IHC	9.988	11.696	10.80	10.67	11.2
CSIR	10.718	9.178	9.92	13.51	8.7
RO	2.479	2.02	2.24	4.5	3.7

The comparison of *Sa* (5% damping) for simulated and observed ground motions at different sites in the Delhi region during the Chamoli earthquake is shown in Figure 15. It is observed that *Sa* for simulated ground motion at CPCB, IHC CSIR, and RO sites match satisfactorily with *Sa* for the observed ground motion. But at sites CPCB and CSIR, *Sa* for simulated ground motion is higher than *Sa* of observed ground motion in the time period range 1-2 sec.

For the simulation of the future great earthquake (M_w 7.5, 8.0, and 8.5) in the Delhi region, $\Delta\sigma_G$ and $\Delta\sigma_L$ values of 30 and 180 bars respectively are used. Other seismological parameters are the same as given in Table 2. The contour maps of *PGA* at bedrock level (without site amplification) in the Delhi region of the future great earthquake from (i) hypocenter of the Chamoli earthquake and (ii) other earthquakes originating (30.0°N, 79.2°E) between MBT and MCT are shown in Figure 16 and 17 respectively. It is observed that the *PGA* varies from 0.014g-0.019g for M_w 7.5, 0.022g-0.031g for M_w 8.0 and 0.033g-0.045g for M_w 8.5 earthquakes for hypocenter (i) and it varies from 0.018g-0.027g for M_w 7.5, 0.027g-0.040g for M_w 8.0, 0.041g-0.061g for M_w 8.5 earthquakes for hypocenter (ii).

Earlier Singh et al. [10]) had predicted *PGA* in the Delhi region at bedrock level from possible future/large great earthquakes (M_w 7.5, 8.0, 8.5) from locations stated above. The simulated *PGA* values at the RO site using a specific barrier model and stochastic finite fault method (Singh et al. [10]) are compared in Table 6. It is observed that *PGA* values simulated using the specific barrier model are higher than the *PGA* values simulated using the stochastic finite fault method. In this regard, it may be noted in Table 5 that the simulated *PGA* value using a specific barrier model is higher than the value simulated using the stochastic finite fault method at RO.

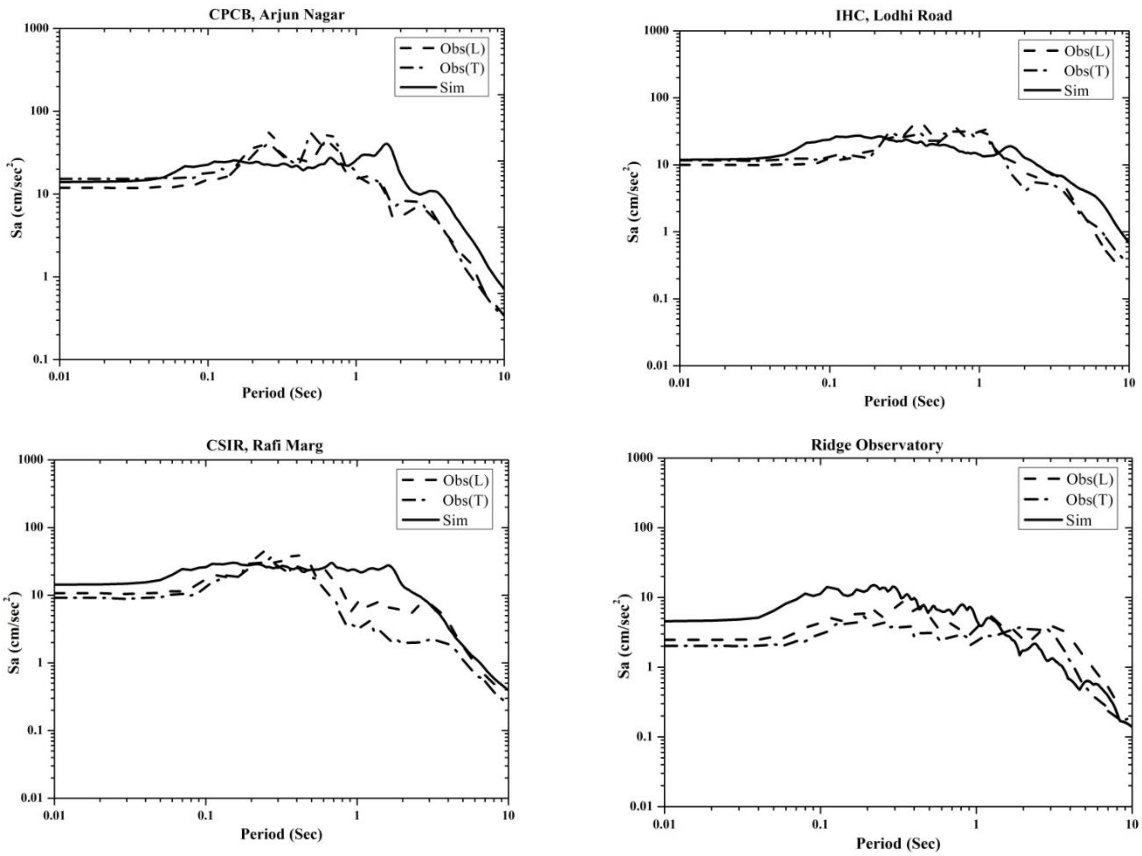

Fig. 15 Comparison of simulated and observed *Sa* (5% damping) at different sites in the Delhi region during the Chamoli earthquake

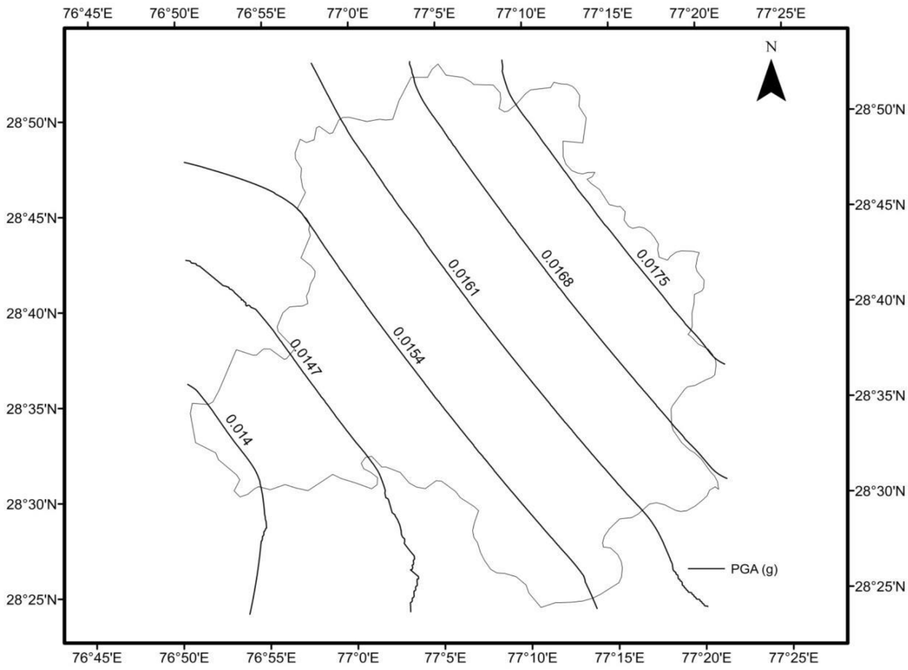
76°45'E
76°50'E
76°55'E
77°0'E
77°5'E
77°10'E
77°15'E
77°20'E
77°25'E
28°50'N
28°45'N
28°40'N
28°35'N
28°30'N
28°25'N
N
0.0175
0.0168
0.0161
0.0154
0.0147
0.014
PGA (g)

(a)

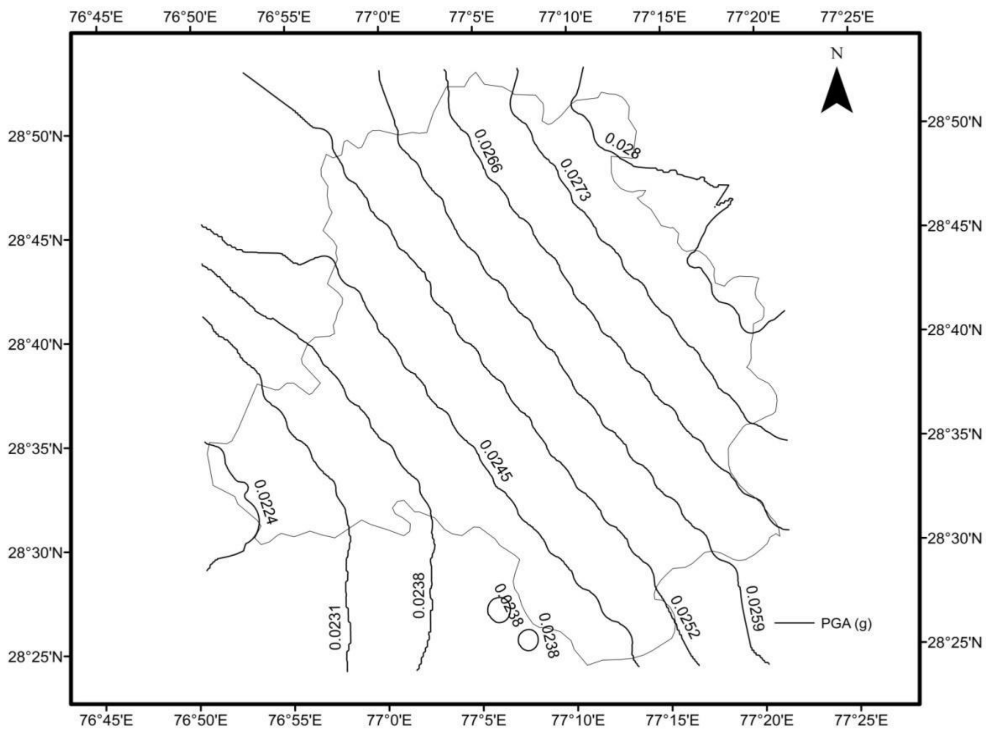
76°45'E
76°50'E
76°55'E
77°0'E
77°5'E
77°10'E
77°15'E
77°20'E
77°25'E
28°50'N
28°45'N
28°40'N
28°35'N
28°30'N
28°25'N
N
0.028
0.0273
0.0266
0.0245
0.0224
0.0231
0.0238
0.0238
0.0238
0.0252
0.0259
PGA (g)

(b)

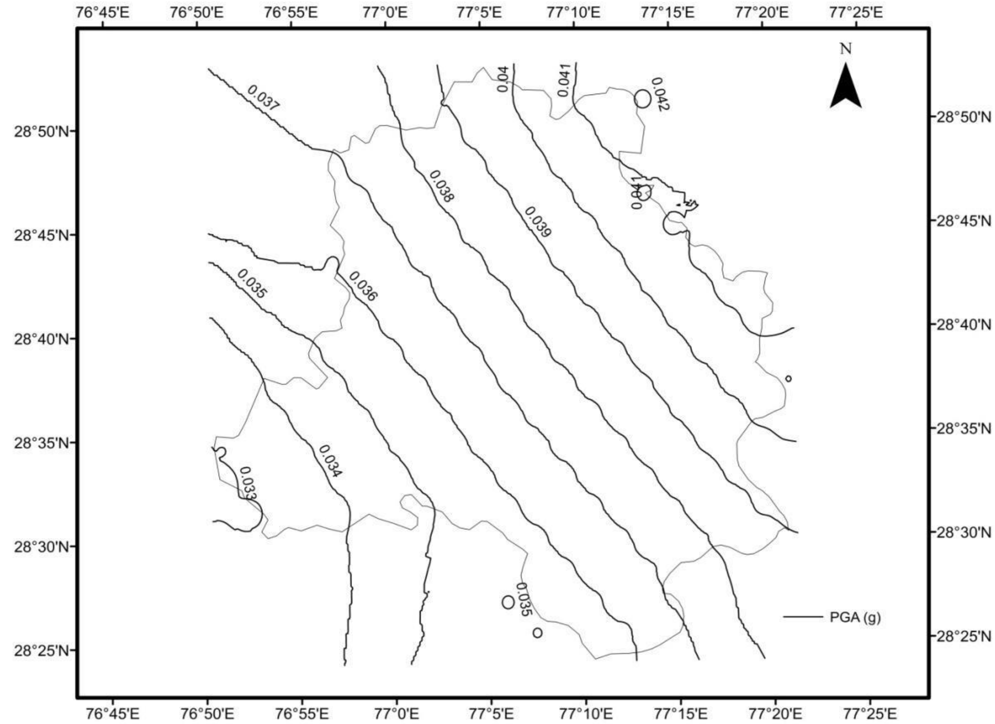

(c)

Fig. 16 The distribution of PGA (g) from an (a) M_w 7.5, (b) M_w 8.0 and (c) M_w 8.5 scenario earthquakes with hypocenter of Chamoli earthquake

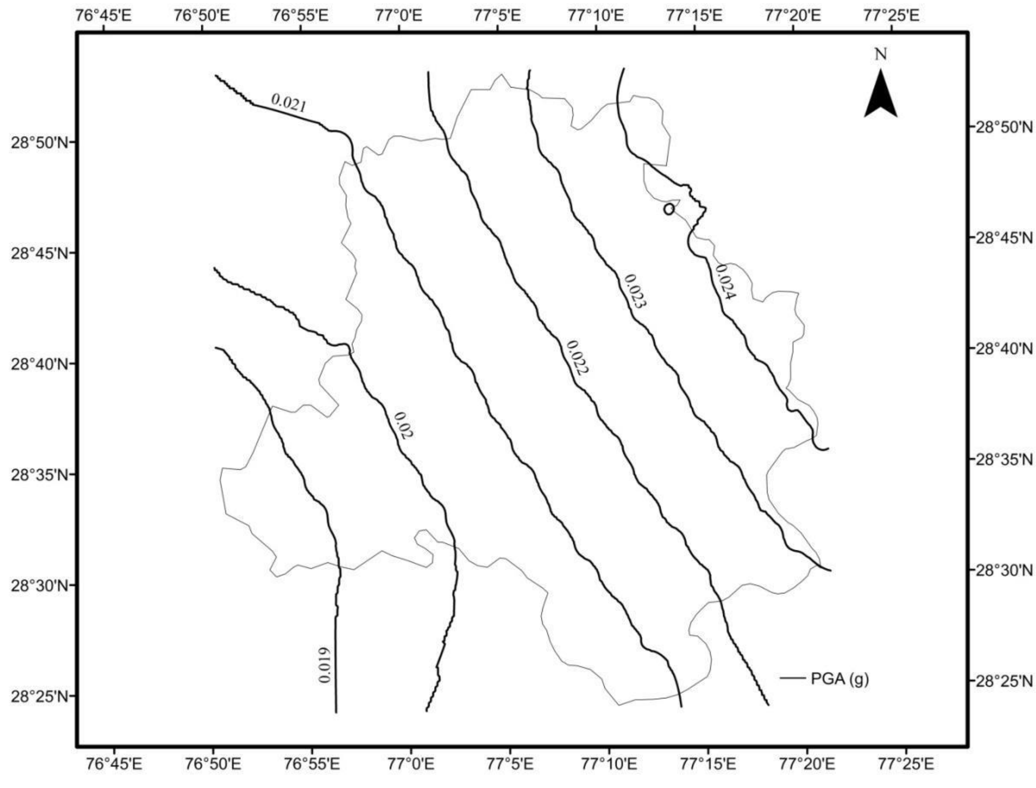

(a)

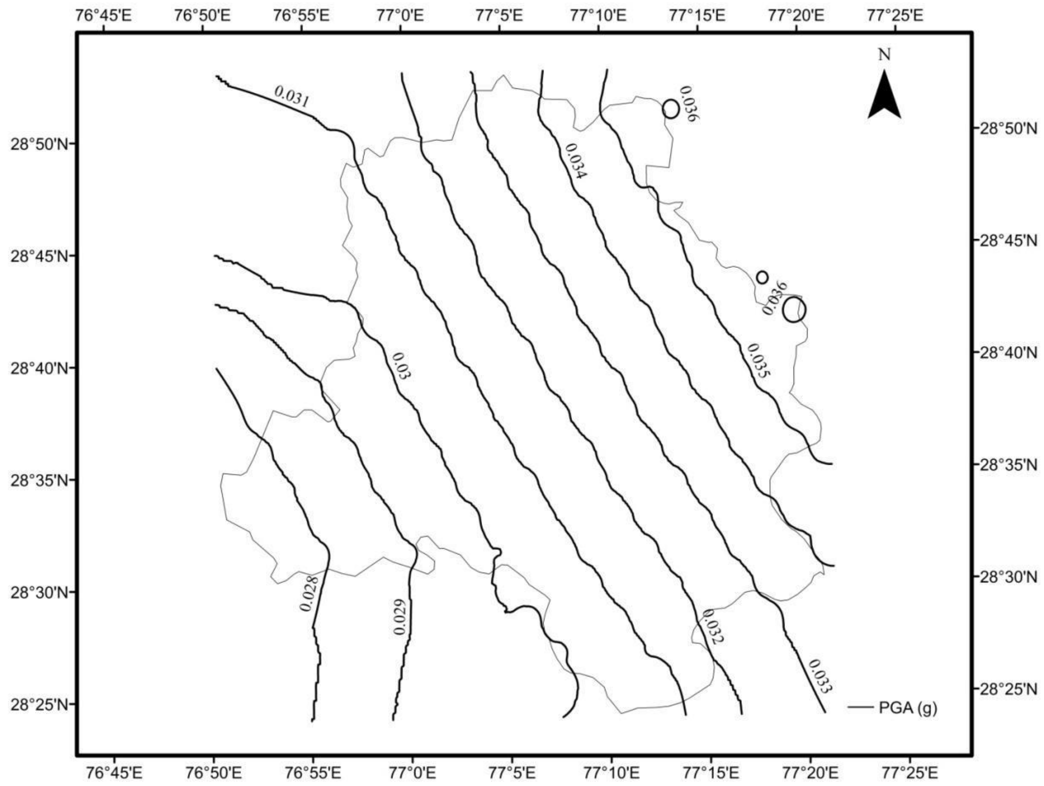

(b)

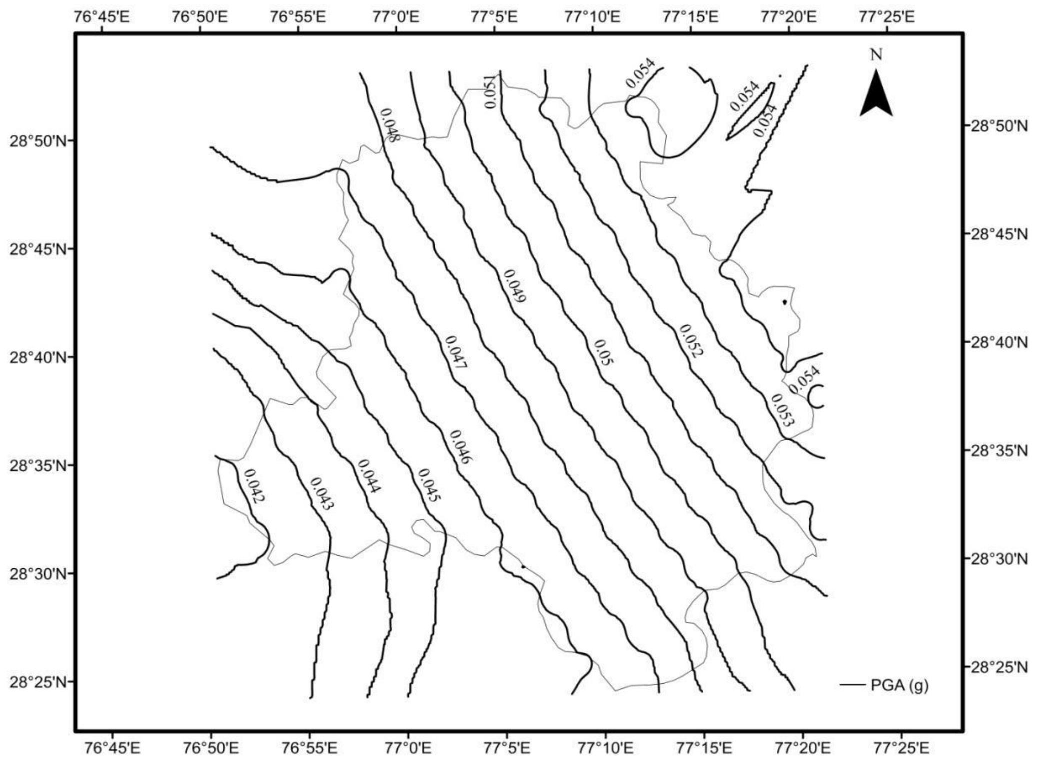

(c)

Fig. 17 The distribution of PGA (g) from an (a)M_w 7.5, (b) M_w 8.0 and (c) M_w 8.5 scenario earthquakes originating (30.0°N, 79.2°E) between MBT and MCT

Table 6: Comparison of PGA (cm/sec^2) value at RO in the Delhi region

Hypocenter	M_w	Present Study	Singh et al. [10]
Chamoli earthquake	7.5	15.50	11.8
	8.0	23.11	19.6
	8.5	35.40	32.9
Center at 30.0°N, 79.2°E	7.5	20.16	15.4
	8.0	29.68	27.7
	8.5	45.22	47.6

Chopra et al. [17] predicted *PGA* to be about 80 cm/sec^2 at the base rock with V_{S30} (620 m/sec) in the Delhi region using a stochastic finite fault method based on dynamic corner frequency for M_w 8.5 earthquake from the hypocenter (i). In the present study, the *PGA* value estimated by Chopra et al. [17] is two times higher than the simulated *PGA* value at RO (without site amplification) using a specific barrier model. The amplification factor for sites with V_{S30} (620 m/sec) is around 2 times the amplification factor for a very hard rock site (Boore and Joyner [53]). *Sa* for 5% damping at RO for M_w 7.5, 8.0, and 8.5 future earthquakes from the hypocenter (i) and (ii) is shown in Figure 18.

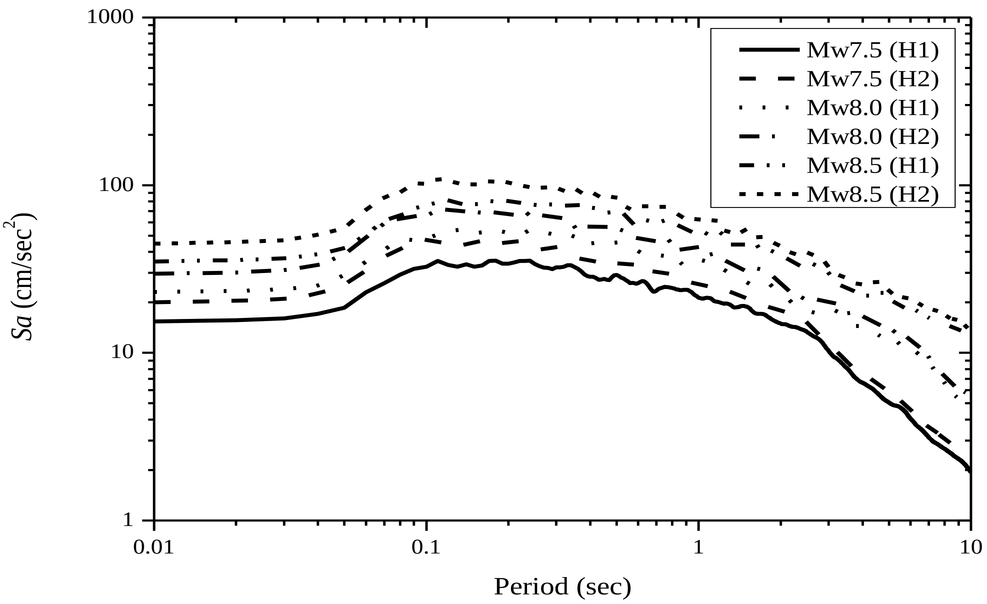

Fig. 18 *Sa* response spectra (5% damping) at Ridge Observatory for M_w 7.5, 8.0, and 8.5 earthquakes from the hypocenter (i), H1 and (ii), H2

CONCLUSIONS

The specific barrier model has been used to simulate the Uttarkashi and Chamoli earthquakes in the Himalayan region. Calibration of $\Delta\sigma_G$ and $\Delta\sigma_L$ parameters of specific barrier model using genetic algorithm has been carried out by comparing the simulated with observed ground motions. The available attenuation/diminution filters, κ_o and f_{max} have been used. $\Delta\sigma_G$ and $\Delta\sigma_L$ values are found to be 30 bars and 180 bars respectively for the f_{max} filter and 30 bars and 510 bars respectively for the κ_o filter. Significantly different values of $\Delta\sigma_L$ are obtained from the two filters. Although $\Delta\sigma_L$ for two filters is different, but *Sa* for two filters is close. The f_{max} filter with the least root means square has been used for the simulation of ground motion. The simulated *Sa* and *PGA* values have shown a similar trend with observed values in the Himalayan region. The discrepancy between the simulated and observed *Sa* and *PGA* values may be due to the local site effect.

The comparison between simulated and observed *PGA* and *Sa* for the Chamoli earthquake was recorded at CPCB, IHC, CSIR, and Ridge Observatory sites in the Delhi region. The simulated *PGA* using a specific barrier model gave closer results at two sites from four sites than the predicted *PGA* using the stochastic finite fault method. The *Sa* for simulated and observed ground motion matches satisfactorily at four stations. For the assessment of various simulation procedures needed more recorded data. The specific barrier model with estimated parameters ($\Delta\sigma_G$ and $\Delta\sigma_L$) has been used to simulate the future great earthquakes (M_w 7.5, 8.0, and 8.5) in the Delhi region at bedrock level from the hypocenter lies between MBT-MCT (centered at 30.0^0N, 79.2^0E) and Chamoli earthquake hypocenter. Results are presented in terms of the contour map of *PGA*. These ground motions can be further combined with local soil conditions and then used for the nonlinear seismic response of structures in the Delhi region.

REFERENCES

1. Rajendran, K. and Rajendran, C.P. (2011). “Revisiting the Earthquake Source in the Himalaya: Perspectives on Past Seismicity”, *Tectonophysics, Vol. 504, pp. 75-88*.
2. Khattri, K.N. and Tyagi, A.K. (1983). “Seismicity Patterns in the Himalayan Plate Boundary and Identification of the Areas of High Seismic Potential”, *Tectonophysics, Vol. 96, pp. 281-297*.
3. Khattri, K. (1987). “Great Earthquakes, Seismicity Gaps and Potential for Earthquake Disaster along the Himalaya Plate Boundary”, *Tectonophysics, Vol. 138, pp. 79-92*.
4. Feld, N. and Bilham, R. (2006). “Great Himalayan Earthquakes and the Tibetan Plateau”, *Nature, Vol.* 444*, pp. 165-170*.
5. Bilham, R. and Ambraseys, N. (2005). “Apparent Himalayan Slip Deficit from the Summation of Seismic Moments for Himalayan Earthquakes, 1500-2000”, *Current Science, Vol. 88, pp. 1658-1663*.
6. Bilham, R. and Wallace, K. (2005). “Future M_w>8 Earthquakes in the Himalaya: Implications from the 26thDec. 2004,M_w = 9.0 Earthquake on India’s Eastern Plate Margin”, *Geological Survey of India Special Publication, Vol. 85, pp. 1-4*.
7. Khattri, K.N. (1999). “An Evaluation of Earthquakes Hazard and Risk in Northern India”, *Himalaya Geology, Vol. 20, pp. 1-46*.
8. Mondal, S.K., Borghi. A., Roy. P.N.S. and Aoudia, A. (2016). “GPS, Scales Exponent and Past Seismicity for Seismic Hazard Assessment in Garhwal-Kumaun, Himalayan Region”, *Natural Hazards, Vol. 80, pp. 1349-1367*.
9. Bilham, R., Gaur, V.K. and Molnar, P. (2001). “Himalayan Seismic Hazard”, *Science Vol. 293, pp. 1442, DOI: 10.1126/science.1062584.*
10. Singh, S.K., Mohanty, W.K., Bansal, B.K. and Roonwal, G.S. (2002). “Ground Motion in Delhi from Future Large/Great Earthquakes in the Central Seismic Gap of the Himalayan Arc”, *Bulletin of Seismological Society of America, Vol. 92, pp. 555-569*.
11. Joshi, A. (2003). “Predicting Strong Motion Parameters for the Chamoli Earthquake of 28th March 1999, Garhwal Himalaya, India, from Simplified Finite Fault Model”, *Journal of Seismology, Vol. 7, pp. 1-17*.
12. Anbazhagan, P., Kumar, A. and Sitharam, T.G. (2013). “Ground Motion Prediction Equation Considering Combined Dataset of Recorded and Simulated Ground Motions”, *Soil Dynamics and Earthquake Engineering, Vol.* 53, pp. 92-108.
13. Harbindu, A., Sharma, M.L. and Kamal (2011). “Stochastic Ground Motion Simulation of Two Himalayan Earthquakes: Seismic Hazard Assessment Perspective”, *Journal of Seismology, https//doi 10.1007/s10950-011-9247-6*.
14. Harbindu, A., Gupta, S. and Sharma, M.L. (2014). “Earthquake Ground Motion Predictive Equations for Garhwal Himalaya, India”, *Soil Dynamics and Earthquake Engineering, Vol. 66, pp. 135-148*.
15. Sharma, B., Chopra, S., Sutar, A.K. and Bansal, B.K. (2013). “Estimation of Strong Ground Motion from a Great Earthquake M_w 8.5 in Central Seismic Gap Region, Himalaya (India) using Empirical Green’s Function Technique”, *Pure and Applied Geophysics, DOI 10.1007/s00024-013-0647-0*.
16. Mittal, H. and Kumar, A. (2015). “Stochastic Finite-fault Modeling of M_w 5.4 Earthquake along Uttarakhand-Nepal Border”, *Natural Hazards, Vol. 75, pp. 1145-1166*.

17. Chopra, S., Kumar, V., Suthar, A. and Kumar, P. (2012). "Modeling of Strong Ground Motions for 1991 Uttarkashi, 1999 Chamoli Earthquakes, and a Hypothetical Great Earthquake in Garhwal-Kumaun Himalaya", *Natural Hazards, Vol. 64, pp. 1141-1159*.
18. Yu, G., Khattri, K.N., Anderson, J.G., Brune, J.N. and Zeng, Y. (1995). "Strong Ground Motion from the Uttarkashi, Himalaya, India, Earthquake: Comparison of Observations with Synthetics using the Composite Source Model", *Bulletin of Seismological Society of America, Vol. 85, pp. 31-50*.
19. Mohan, K. and Joshi, A. (2013). "Simulation of Strong Ground Motion due to Great Earthquake in the Central Seismic Gap Region of Uttarakhand Himalaya", *Natural Hazards, Vol. 69, pp. 1733-1749*.
20. Bresnev, I.A. and Atkinson, G.M. (1997). "Modeling Finite Fault Radiation from the ω^n Spectrum", *Bulletin of Seismological Society of America, Vol. 87, pp. 67-84*.
21. Boore, D.M. and Atkinson, G.M. (1987). "Stochastic Prediction of Ground Motion and Spectral Response Parameters at Hard Rock Sites in Eastern North America", *Bulletin of Seismological Society of America, Vol. 77, pp. 440-467*.
22. Papageorgiou, A.S. (1988). "On Two Characteristics Frequencies of Acceleration Spectra: Patch Corner Frequency and f_{max}", *Bulletin of Seismological Society of America, Vol. 78, pp. 509-529*.
23. Beresnev, I.A. (2001). "What we can and cannot Learn About Earthquake Sources from the Spectra of Seismic Waves", *Bulletin of Seismological Society of America, Vol. 91, pp. 397-400*.
24. Papageorgiou, A.S. and Aki, K. (1983a). "A Specific Barrier Model for the Quantitative Description of Inhomogeneous Faulting and the Prediction of Strong Ground Motion. I Description of the Model", *Bulletin of Seismological Society of America, Vol. 73, pp. 693-722*.
25. Papageorgiou, A.S. and Aki, K. (1983b). "A Specific Barrier Model for the Quantitative Description of Inhomogeneous Faulting and the Prediction of Strong Ground Motion. Part II. Applications of the Model", *Bulletin of Seismological Society of America, Vol. 73, pp. 953–978*.
26. Halldorsson, B. and Papageorgiou, A.S. (2005). "Calibration of the Specific Barrier Model to Earthquakes of Different Tectonic Regions", *Bulletin of Seismological Society of America, Vol.* 95, *pp. 1276-1300*.
27. Papageorgiou, A.S. (2003). "The Barrier Model and Strong Ground Motion", *Pure and Applied Geophysics, Vol. 160, pp. 603-634*.
28. Shrivastava, Hemant (2018). "Site Dependent Seismic Evaluation of Buildings in Delhi Region" *Ph.D. Thesis, Department of Civil Engineering, Indian Institute of Technology Delhi*.
29. Valdiya, K.S. (1980). "The Two Intracrustal Boundary Thrusts of the Himalaya", *Tectonophysics, Vol. 66, pp.323-348*.
30. Ni, J. and Barazangi, M. (1984). "Seismotectonics of the Himalaya Collision Zone: Geometry of the Underthrusting Indian Plate beneath the Himalaya", *J. Geophys Res Solid Earth, Vol.* 89, pp. 1147-1163.
31. Kayal, J.R. (2001). "Microearthquake Activity in Some Parts of the Himalaya and the Tectonic Model", *Tectonophysics, Vol.* 339*, pp. 331-351*.
32. Boore, D.M. (2003). "Simulation of Ground Motion using the Stochastic Method", *Pure and Applied Geophysics, Vol.* 160, pp. 635-676.
33. Aki, K. and Richards, P.G. (1980). "Quantitative Seismology. *Theory and Methods*", *W.H. Freeman, San Francisco*.
34. Beresnev, I.A. and Atkinson, G.M. (2002). "Source Parameters of Earthquakes in Eastern and Western North America Based on Finite-fault Modeling", *Bulletin of Seismological Society of America, Doi.org/10.1785/0120010101*.
35. Borcherdt, R.D. (1970). "Effects of Local Geology on Ground Motion Near San Francisco Bay", *Bulletin of Seismological Society of America, Vol. 60, pp. 29-61*.
36. Nakamura, Y. (1989). "A Method for Dynamic Characteristics Estimation of Subsurface using Micro Tremor on the Ground Surface", *Quarterly Report, Railway Technical Research Institute,Vol. 30, No. 1, pp. 25-33*.
37. Lermo, J. and Chavez-Garcia, F.J. (1993). "Site Effect Evaluation using Spectral Ratios with only One Station", *Bulletin of Seismological Society of America, Vol. 83, pp. 1574-1594*.

38. Motazedian, D. (2006). "Region Specific Key Seismic Parameters for Earthquakes in Northern Iran", *Bulletin of Seismological Society of America, Vol. 96, pp. 1383-1395*.
39. Steidl, J.H., Tumarkin, A.G. and Archuleta, R.J. (1996). "What is a Reference Site?", *Bulletin of Seismological Society of America, Vol. 86, pp. 1733-1748*.
40. Castro, R.R., Rovelli, A., Cocco, M., Bona, M.D. and Pacor, F. (2001). "Stochastic Simulation of Strong Motion Records from the 26th September 1997, (M_w 6), Umbria-Marche (Central Italy) Earthquake", *Bulletin of Seismological Society of America, Vol. 91, pp. 27-39*.
41. Shoja-Taheri, J. and Ghofrani, H. (2007). "Stochastic Finite-fault Modeling of Strong Ground Motions from the 26th December 2003 Bam, Iran, Earthquake", *Bulletin of Seismological Society of America, Vol. 97, pp. 1950-1959*.
42. Holland, J.H. (1975). "Adaptation in Natural and Artificial Systems", *University of Michigan Press, Ann Arbor, Michigan*.
43. Goldberg, D.E. (1989). "Genetic Algorithms in Search, Optimization and Machine Learning", *Addison-Wisely Publishing, Inc., Reading, MA*.
44. Soghart, M.R., Khaji, N. and Zafarani, H. (2012). "Simulation of Strong Ground Motion in Northern Iran Using the Specific Barrier Model", *Geophysical Journal International, Vol.* 188, pp. 645-679.
45. Zafarani, H., Mousavi, M., Noorzad, A.S. and Ansari, A. (2008). "Calibration of the Specific Barrier Model to Iranian Plateau Earthquakes and Development of Physically Based Attenuation Relationships for Iran", *Soil Dynamics and Earthquake Engineering, Vol. 28, pp. 550-576*.
46. Yilmaz, S. (2011). "Ground Motion Predictive Modeling Based on Genetic Algorithms", *Natural Hazards and Earth System Science, Vol. 11, pp. 2781-2789*.
47. Naeim, F., Alimoradi, A. and Pezeshk, S. (2004). "Selection and Scaling of Ground Motion Time Histories for Structural Design using Genetic Algorithms", *Earthquake Spectra, Vol.* 20, pp. 413-426.
48. Coley, D.A. (1999). "An Introduction to Genetic Algorithms for Scientists and Engineers", *World Scientific, Singapore*.
49. Geng, M. and Cheng, R. (1997). "Genetic Algorithms and Engineering Design", *Wiley, New York*.
50. Joshi, A. (2006). "Analysis of Strong Motion Data of the Uttarkashi Earthquake of 20th October 1991 and the Chamoli Earthquake of 28th March 1999 for Determining the Q Value and Source Parameters", *ISET Journal of Earthquake Technology, Vol. 43, pp. 11-29*.
51. Kumar, D., Sarkar, I., Sriram, V. and Khattri, K.N. (2005). "Estimation of the Source Parameters of the Himalaya Earthquake of 19th October, 1991, Average Effective Shear Wave Attenuation Parameter and Local Site Effects from Accelerograms", *Tectonophysics, Vol. 407, pp. 1-24*.
52. Sriram, V. and Khattri, K.N. (1997). "A Study of Source Spectrum, Site Amplification Functions, Response Spectra, Fourier Spectra, and Peak Ground Accelerations from the Strong Ground Motion Data of the 1991 Uttarkashi Earthquake", *Current Science, Vol. 72, pp. 728-740*.
53. Boore, D.M. and Joyner, W.B. (1997). "Site Amplification for Generic Rock Sites", *Bulletin of Seismological Society of America, Vol.* 87, pp. 327-341.